Life Technologies (Grand Island, NY). The characteristics of the human hepatocyte donors are described in **Table S4**. The pharmacokinetic studies using these mice were performed 8-12 weeks after transplantation of the human liver cells. Control NOG mice and humanized TK-NOG mice were administered 25 mg/kg clemizole PO, and blood samples were collected 30 minutes after dosing. The C57BL/6J mice (3 per time point) were dosed with 25 mg/kg PO Clemizole, and blood samples were collected at 15, 30 min and 1, 2, 4 and 6 hrs after dosing for analysis. For the drug-drug interaction studies, eight humanized TK-NOG mice were dosed with Clemizole (25 mg/kg P.O.) with or without ritonavir (20 mg/kg P.O), and blood samples were collected 30 minutes after dosing. Six of these mice were also treated with debrisoquine (10 mg/kg PO), in the presence or absence of ritonavir (20 mg/kg PO), and plasma obtained 2 hrs later for analysis.

Statistical analysis of mouse pharmacokinetic data. To assess the statistical significance of the difference in the relative amount of each metabolite (clemizole, M1, M2, M6, M12, M14 and M15) in plasma obtained from control and humanized TK-NOG mice, a two-sample two-sided t test was used. Of note, the amount of M1 was < 7 in all 8 of the control mice, while it was > 7 in all but one of the humanized TK-NOG mice. The two-sample two-sided t test result indicated that this difference in M1 abundance was highly significant (p value = 0.0004). In the DDI studies, a paired-sample t test was used to compare the amount of each of the metabolites (Figure 2) and for the clemizole AUC (0-12hr) (Figure 3) measured in the presence and absence of ritonavir co-administration. The paired-sample t test was also used to compare the relative amounts of 4-OH debrisoquine in the 6 humanized TK-NOG mice measured in the presence or absence of ritonavir co-administration.

Quantitative analysis of clemizole and metabolites in plasma. Mouse plasma (50 uL) was treated with acetonitrile with 0.1% formic acid (200 uL), vortexed and incubated at -20 ^{0}C for one

hour, centrifuged at 10,000 rpm for 10 min. The supernatants were collected, dried and resuspended in 50uL 5% acetonitrile with 0.1% formic acid for the analysis by LC/MS. HPLC was performed using an Agilent 1200 column compartment, capillary pump, and an autosampler on a Zorbax C18 column, 0.5x150 mm. The flow rate was 20 mL/min with a gradient from 5% solvent B (acetonitrile with 0.1% formic acid; solvent A is 0.1% formic acid in water) to 95% B in 30 min and held at 95% B for 5 min. Mass spectrometric analysis were carried out on an Agilent Model 6520 qTOF mass spectrometer equipped with an ESI source. The heated capillary temperature in the source was held at 325°C. Full scan (m/z 110–1000) spectra or data dependent MS/MS spectra were collected. The metabolites were identified based on their collision-induced dissociation behavior in tandem mass spectrometry, accurate mass and retention time. Quantitative analysis of clemizole was performed using a calibration curve at 9-1257 ng/ml clemizole spiked into blank mouse plasma and extracted as above. An internal standard 1-(p-bromobenzyl)-2-(1-pyrrolidinylmethyl)- Benzimidazole was also spiked in at 1000ng/ml. Relative amounts of clemizole and metabolites in each sample were calculated using the assumption that all compounds had the same MS response factor.

Human pharmacokinetic and metabolite studies. Phase 1b studies (to be reported elsewhere) were conducted in genotypes 1 and 2 HCV patients under IRB-approved protocols to investigate the safety and tolerability, pharmacokinetics, and pharmacodynamics of clemizole HCl (see www.Clinicaltrials.gov and approval by the University of Ankara Medical School Ethics Committee; study sponsor Eiger BioPharmaceuticals, Inc.). De-identified aliquots of excess material, which were not needed for clinical monitoring, were kindly provided by Wenjin Yang (Eiger BioPharmaceuticals, Inc.) to us for PK and metabolite analysis. The samples obtained were from human subjects that were administered 100 mg Clemizole P.O., with or without 100 mg ritonavir P.O. administered one hour before the clemizole, and blood samples were obtained 0 to 12 hrs after dosing. The relative abundance of clemizole and its metabolites in plasma

were measured in samples obtained from 10 patients treated with clemizole alone, and from 3 patients who participated in the subcomponent evaluating the effect of ritonavir co-administration, by LC/MS analysis as described below.

Microsome incubations and analysis. Clemizole (20 uM, diluted from 10 mM stock in DMSO) was mixed with human, rat or mouse liver microsomal proteins (1 mg/ml) in 100 mM potassium phosphate buffer (pH 7.4) supplemented with 1 mM glutathione and 5 mM $MgCl_2$ in a total volume of 1 ml. After 5 min pre-incubation at 37°C, the reactions were initiated by addition of 2 mM NADPH, and then quenched by addition of 1 mL ice cold acetonitrile after 60 min. Negative control samples contained NADPH with test compound added with the acetonitrile quench. HPLC was performed using an Agilent 1200 column compartment, capillary pump, and autosampler on a Zorbax C18 column, 0.5x150 mm. The flow rate was 20 μL/min with a gradient from 5% solvent B (acetonitrile with 0.1% formic acid; solvent A is 0.1% formic acid in water) to 95% B in 30 min and held at 95% B for 5 min. Mass spectrometric analysis were carried out on an Agilent Model 6520 quantitative Time Of Flight mass spectrometer equipped with an ESI source. The heated capillary temperature in the source was held at 325°C. Full scan (m/z 110–1000) spectra or data dependent MS/MS spectra were collected. The metabolites were identified based on their collision-induced dissociation behavior in tandem mass spectrometry, accurate mass and retention time. Relative amounts of clemizole and metabolites in each sample were calculated using the assumption that all compounds had the same MS response factor.

Hepatocyte incubations. Using wide-bore pipette tips, aliquot 0.1 mL cell suspension into a 24 well plate, and the plates were incubated for at least 0.5 hr in a 37 °C incubator on shaker (500 rpm). Two wells of volume 0.5 mL were run for each test compound. Incubation mixtures (0.5 mL) contained test compound (20 uM with a maximum of 1% dimethyl sulfoxide used as

cosolvent) in Gibco HepatoZYME (Invitrogen, Carlsbad, CA, USA) media supplemented with 5% fetal bovine serum and 2mM L-glutamine and were allowed to react for 4 h. All incubations were quenched with an equal volume of acetonitrile, the duplicate wells combined, followed by centrifugation, evaporation to dryness and reconstitution in 10% acetonitrile in water. Negative control samples contained test compound only added with the acetonitrile quench. HPLC was performed using an Agilent (Santa Clara, CA, USA) 1100 column compartment, binary pump, autosampler and diode-array detector on a Varian (Palo Alto, CA, USA) Polaris 5 micron, C18-A column, 2.1x250 mm, in a column heater at 55°C. The flow rate was 0.3 mL/min with a gradient from 0%(after a 5 min hold) solvent B (acetonitrile with 0.1% formic acid; solvent A is 0.1% formic acid in water) to 30% B in 25 min and held at 95% B for 5 min. Mass spectrometric analysis were carried out on a Thermo-Fisher (San Jose, CA, USA) LTQ Orbitrap mass spectrometer equipped with an ESI source. The heated capillary temperature in the source was held at 250°C. Full scan positive spectra were collected along with MS/MS spectra for the major two peaks with the Orbitrap. Corresponding positive ion MS^3 spectra were collected with the LTQ low resolution detector. Negative full scan (m/z 180–900), MS/MS and MS^3 spectra were collected with the LTQ low resolution detector. Relative quantitative analyses were based on UV integration (276 nm) of identified peaks.

CYP reaction phenotyping. The reaction phenotyping was conducted using cDNAs expressing recombinant hCYP450 enzymes. (rhCYP 1A2, 2C8, 2C9, 2C19, 2D6, 3A4) and control preparations from baculovirus-infected Sf9 insect cells (supersomes) that were purchased from BD Gentest (Woburn, MA). Cytochrome c reductase was co-expressed in all preparations, and cytochrome b5 was expressed in cDNA-expressed CYP2C8, 2C9, 2C19, and 3A4. Incubation mixtures were prepared containing potassium phosphate buffer (50 mM, pH 7.4), magnesium chloride (5 mM), rhCYP450 enzymes (varied CYP concentration at pmole/ml with total 0.5 mg protein/ml), and clemizole (1 μM). The reaction mixtures were pre-incubated at 37°C for five

minutes prior to initiation of reactions with NADPH (2 mM final concentration) and stopped by addition of acetonitrile (1:1 by volume) at pre-determined time points (0, 5, 10, 20 min). Following quenching, one volume of sample was transferred to an injection plate containing one volume acetonitrile/water with internal standard. Samples were centrifuged at 3000 rpm for 10 min and the supernatants were collected for the analysis by LC/MS. Quantitative analysis of clemizole depletion was conducted using LC/MS/MS on an ABI 4000 mass spectrometer using MRM (mz 326 to m/z 255) with sample introduction on LC system containing a Shimadzu 20ADP binary pumps (Columbia, MD) and HTC PAL autosampler (Leap Technologies, Cary, NC), and a Hypersil C18 column(2.1x50 mm). The flow rate was 0.4 mL/min with a gradient from 5%(after a 1 min hold) solvent B (Acetonitrile: Methanol (50:50) with 0.1% Formic Acid) and 95% solvent A (5 mM Ammonium Acetate with 0.1% Formic Acid) to 90% B in 3 min and held at 90% B for 1 min. Formation of predicted metabolites (m/z 326 to m/z 255 for parent; 340 to 255 for M1;342 to 271 for M4; 324 to 255 for M2) were monitored on ABI 4000 QTrap mass spectrometer using the using multiple reaction monitoring triggered enhanced product ion scanning to obtain representative MS/MS spectra for the major metabolites (MRM-EPI). The LC method is similar as previously described, except for the column and run time. A Hypersil C18 column, 2.1x100mm, was used and total run time is 25 min.

Supplemental References

Chiu SH, Huskey SW (1998) Species differences in N-glucuronidation. Drug Metab Dispos 26:838-847.

Danielson PB (2002) The cytochrome P450 superfamily: biochemistry, evolution and drug metabolism in humans. Curr Drug Metab 3:561-597.

Fitch WL, He L, Tu YP, Alexandrova L (2007) Application of polarity switching in the identification of the metabolites of RO9237. Rapid Commun Mass Spectrom 21:1661-1668.

Hasegawa M, Kawai K, Mitsui T, Taniguchi K, Monnai M, Wakui M, Ito M, Suematsu M, Peltz G, Nakamura M, Suemizu H (2011) The reconstituted 'humanized Liver' in TK-NOG mice is mature and functional. Biochem Biophys Res Commun 405:405-410.

Proctor NJ, Tucker GT, Rostami-Hodjegan A (2004) Predicting drug clearance from recombinantly expressed CYPs: intersystem extrapolation factors. Xenobiotica 34:151-178.

Supplemental Table 1. LC/MS Characterization of clemizole and its metabolites. The retention times were measured using the hepatocyte LC method, and were adjusted for those few metabolites that were only detected *in vivo* or after incubation with microsomes.

Metabolite	Retention time	Nominal $[M+H]^+$	PPM error	Indicative MS/MS fragments	Indicative MS^3 fragments
Clemizole	14.0	326	2.8	255,125	220
M1	15.2	340	1.8	255,125	
M2	13.2	324	2.8	255,125	
M3	12.8	272	0.7	255,125	
M4	12.2	342	0.3	271,255	
M5	12.7	273	1.1	255,125	
M6	13.3	358	1.1	340,125	255
M7	14.0	356	2.2	338,255,125	
M8	11.7	289	2.4	271,259,125	
M9	12.5	356	0.6	271,125	
M10	13.9	342	1.2	256,257,125	
M11	11.2	288	1.7	271,125	
M12	12.5	243	1.6	125	
M13	10.8	502	2.4	326	255
M14	10.6	518	2.5	342	271,125
M15	11.3	532	2.4	356	271,125
M16	12.6	532	1.9	338	255,125
M17	11.8	449	2.6	273	255,125
M18	10.6	548	2.1	530	372,271
M19	10.4	332*	0.2	356	271,125

Supplemental Table 2. The amount of clemizole and metabolites present after 20 mM clemizole was incubated with human, rat or mouse liver microsomes for 1 hr; or after incubation with rat or human hepatocytes for 30 minutes. The number indicates the % of the total identified metabolites. None of these metabolites were detected in control incubations. ND indicates that a metabolite was not detected

	Microsomes			Hepatocytes	
	Human	**Rat**	**Mouse**	**Human**	**Rat**
Clem	40.1	3	24.1	15	ND
M1	35.5	3.5	2.5	39	ND
M2	1.8	3.5	4.8	0.1	ND
M3	4.6	6.1	5.7	0.2	ND
M4	5.4	4.8	3.4	4	ND
M5	4	6.8	2.5	0.5	ND
M6	2.3	2.7	1.8	18	ND
M7	1	5.3	0.7	4.7	ND
M8	0.3	17.9	9.8	ND	ND
M9	2.9	37.1	19.2	4	1.1
M10	1.3	ND	ND	ND	3.7
M11	0.2	9.3	25.5	ND	ND
M12	0.6	ND	ND	1.2	1.1
M13	ND	ND	ND	3	ND
M14	ND	ND	ND	10	5.4
M15	ND	ND	ND	0.3	43.6
M16	ND	ND	ND	ND	13.1
M17	ND	ND	ND	ND	10.2
M18	ND	ND	ND	ND	10.9
M19	ND	ND	ND	ND	10.9

Supplemental Table 3. The identified metabolites present after incubation of the indicated concentration of 10 uM clemizole with the indicated expressed recombinant human CYP450 for 20 min. The minor Phase 1 metabolites M5-M12 were not observed in the CYP450 phenotyping experiments.

CYP450:	1a2	2b6	2c8	2c9	2c19	2d6	3a4
Metabolites:	M2	M2	M2	M2	M2	M1	M1
	M4			M4		M2	M2

Supplemental Table 4. The age and sex of the 6 different human hepatocyte donors whose cells were used to produce 8 chimeric mice are shown, along with the human serum albumin level measured at the time when the pharmacokinetic experiments were performed. The percentage of the liver that is humanized, which was calculated based upon the measured albumin level as described in (Hasegawa et al., 2011), is also indicated.

Human	Donor		Hu Alb	Human
Mouse #	Age	Sex	(mg/ml)	Liver (%)
1	4	F	4.2	42
2	34	M	1.5	15
3	4	F	1.6	16
4	34	M	2.2	22
5	52	F	2.7	27
6	49	F	1.3	13
7	23	M	7.0	70
8	57	M	1.6	16

Supplemental Figure Legends

Supplemental Figure 1. The top graphs show the measured plasma clemizole concentration at the indicated times after a single oral 25 mg/kg dose of clemizole was administered to Balb/c or NOG mice (4 mice per group). The bottom graphs show the relative normalized abundance of clemizole and metabolites in plasma at the indicated time after dosing. As was observed in C57BL6 mice, clemizole was rapidly metabolized to 2 (M12 and M14) metabolites, while only minimal amounts of M1 or M6 were produced. The metabolite structures are shown in Figure 2.

Supplemental Figure 2. Reconstructed LC/MS chromatograms showing the relative amounts of clemizole and metabolites present after incubation of 20 uM clemizole with human, rat or mouse liver microsomes for 60 minutes. The peaks for clemizole (P), and the major human (M1) or rodent (M8, M9) metabolites are indicated.

Supplemental Figure 3. The % of clemizole remaining after 1 uM clemizole was incubated with control insect cells or with insect cells expressing the indicated recombinant CYP450 enzymes for 20 min.

Supplemental Figure 4. The relative amount of M1 produced after 20 uM clemizole was incubated with human liver microsomes in the presence of the indicated concentrations of ritonavir or omiprazole for 60 minutes.

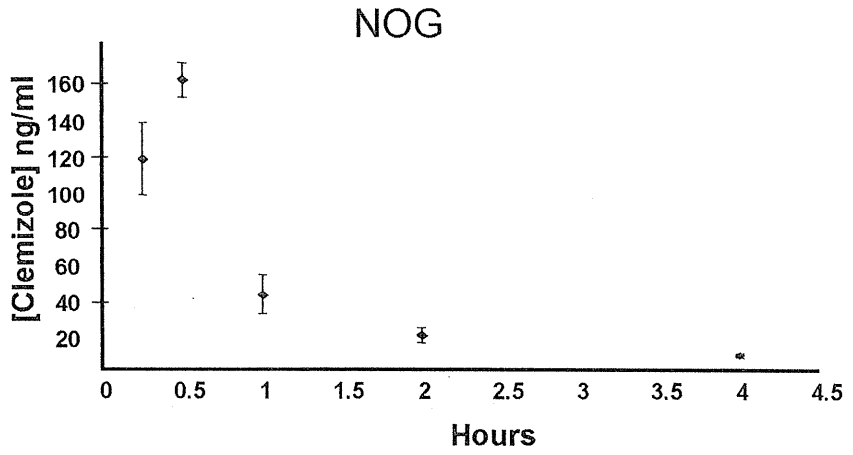
NOG
[Clemizole] ng/ml
160
140
120
100
80
60
40
20
0
0.5
1
1.5
2
2.5
3
3.5
4
4.5
Hours

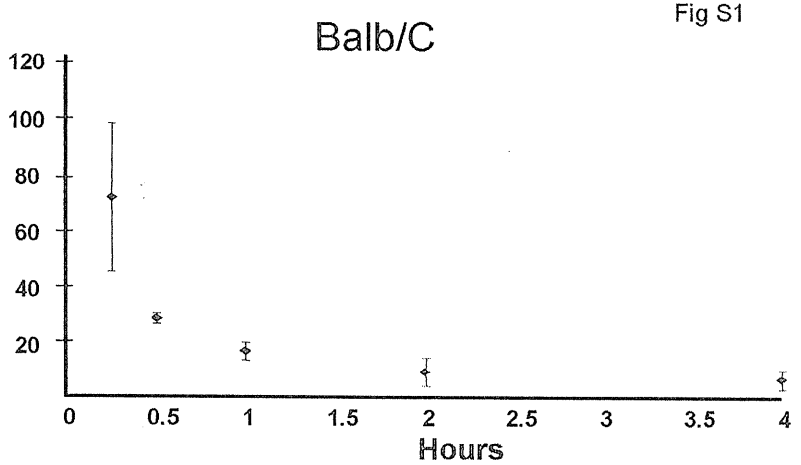
Balb/C
120
100
80
60
40
20
0
0.5
1
1.5
2
2.5
3
3.5
4
Hours

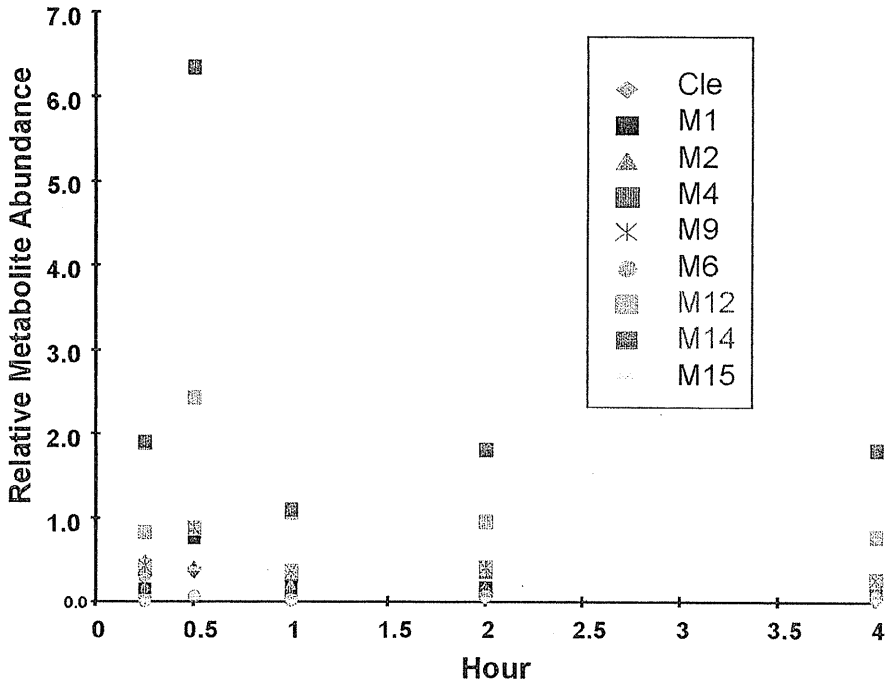
Relative Metabolite Abundance
7.0
6.0
5.0
4.0
3.0
2.0
1.0
0.0
0
0.5
1
1.5
2
2.5
3
3.5
4
Hour
Cle
M1
M2
M4
M9
M6
M12
M14
M15

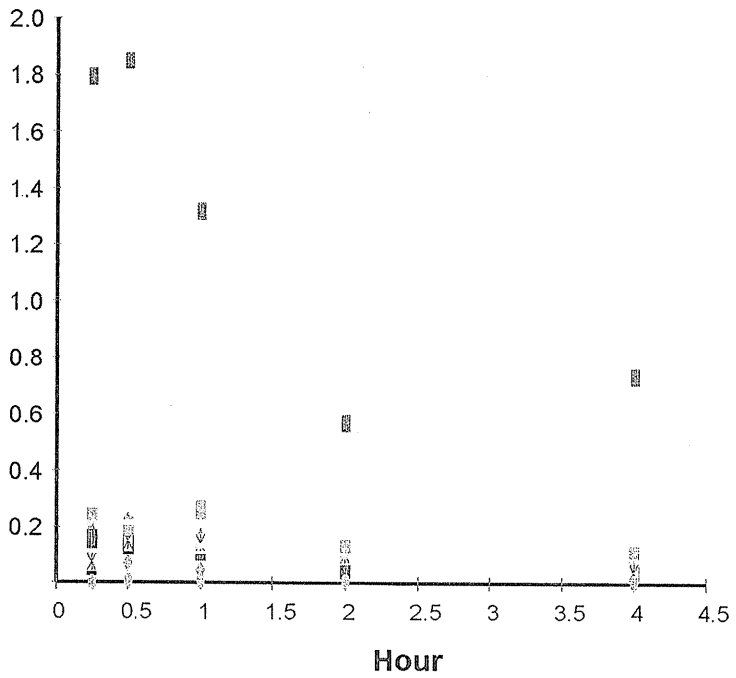
2.0
1.8
1.6
1.4
1.2
1.0
0.8
0.6
0.4
0.2
0
0.5
1
1.5
2
2.5
3
3.5
4
4.5
Hour

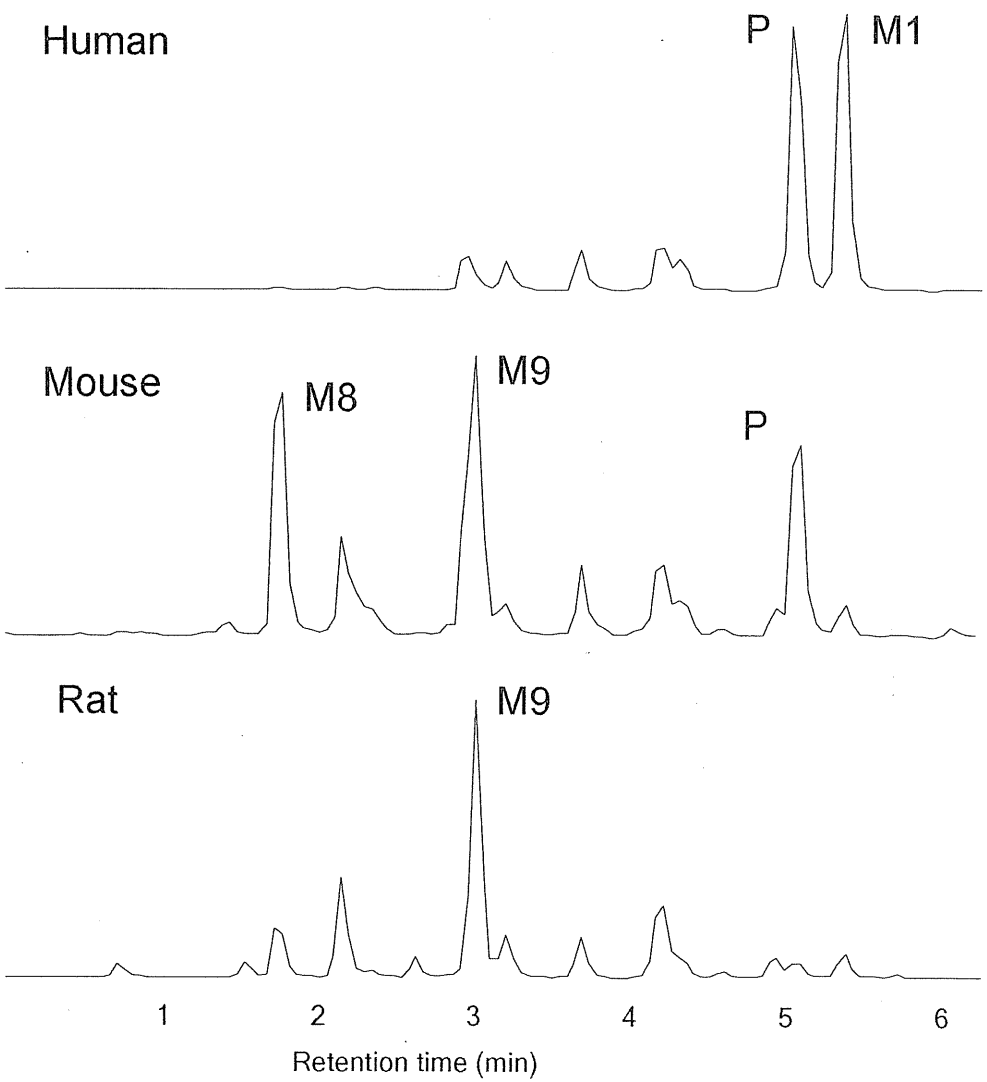
Human
P
M1
Mouse
M8
M9
P
Rat
M9
1
2
3
4
5
6
Retention time (min)

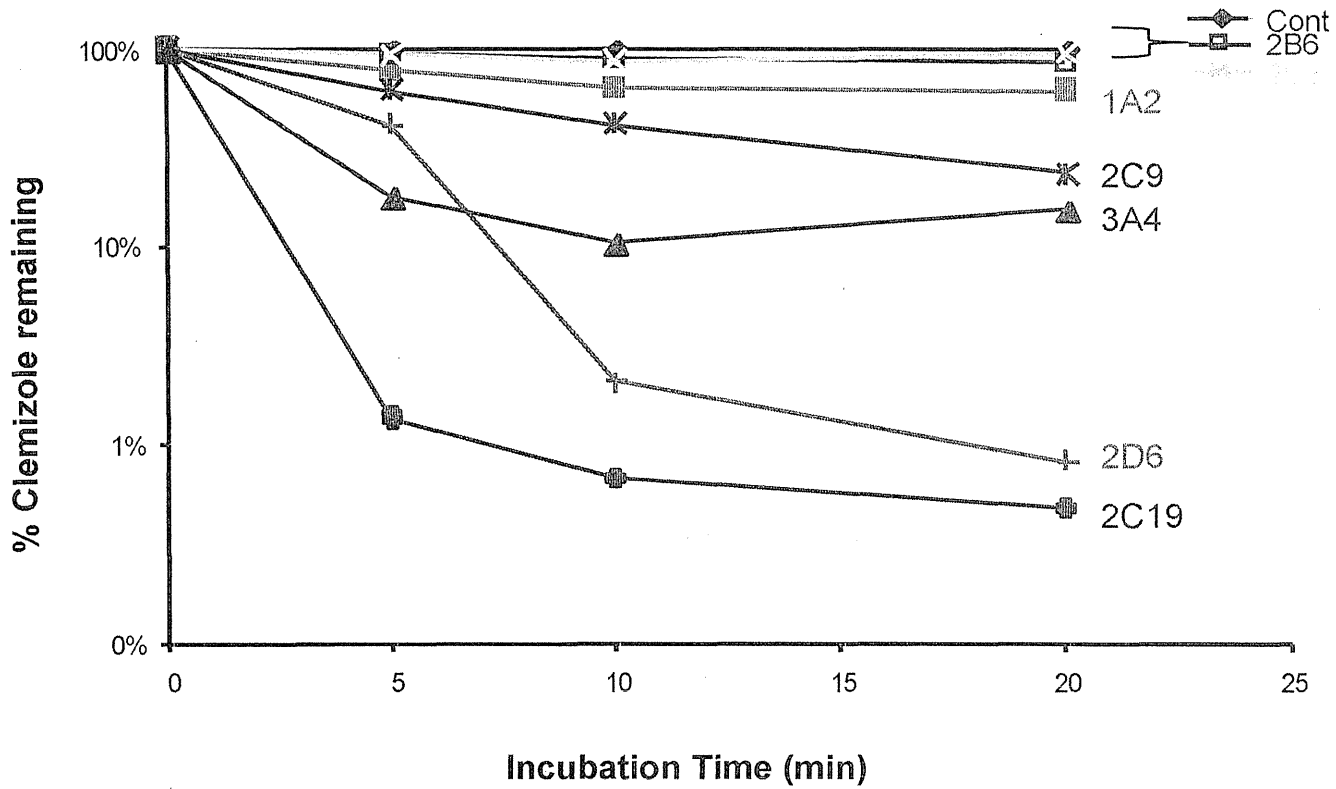
Cont
2B6
1A2
2C9
3A4
2D6
2C19
100%
10%
1%
0%
0
5
10
15
20
25
% Clemizole remaining
Incubation Time (min)

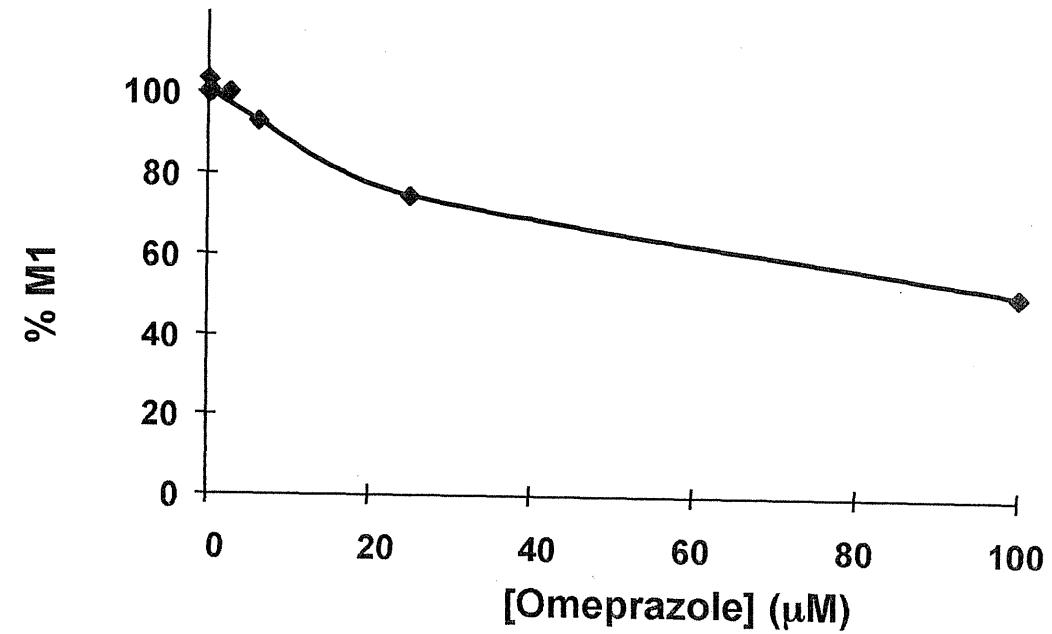
% M1
100
80
60
40
20
0
0
20
40
60
80
100
[Omeprazole] (μM)

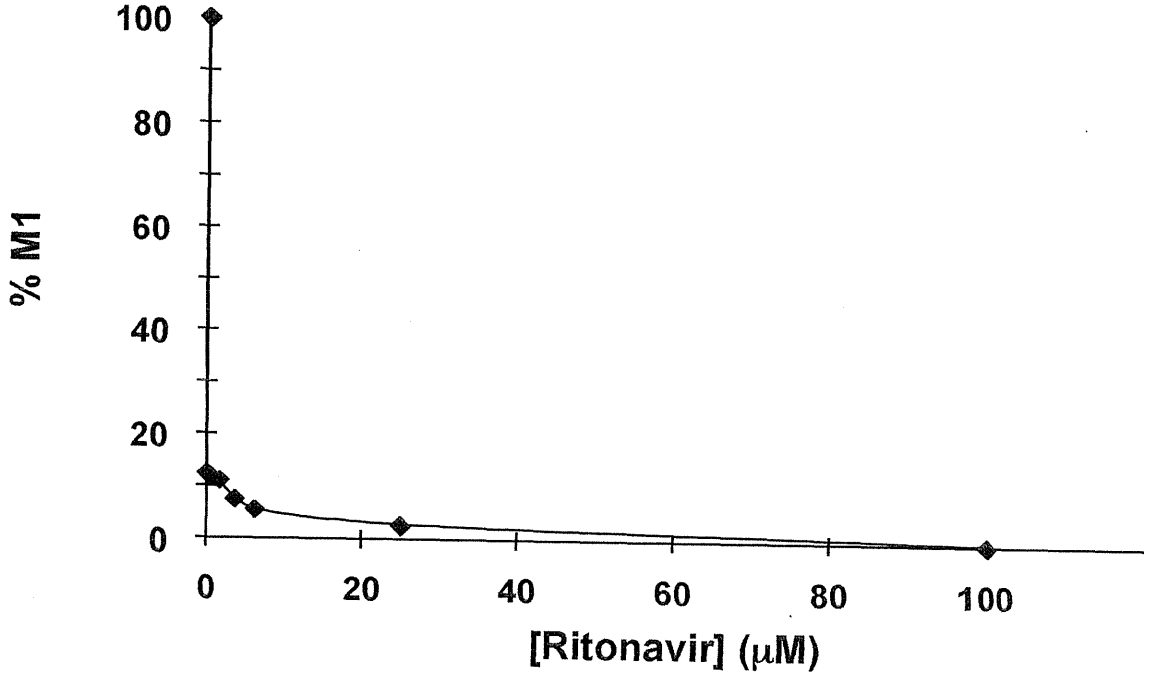
% M1
100
80
60
40
20
0
0
20
40
60
80
100
[Ritonavir] (μM)

Efficient Xenoengraftment in Severe Immunodeficient NOD/Shi-*scid* IL2rγ^{null} Mice Is Attributed to a Lack of CD11c$^+$B220$^+$CD122$^+$ Cells

Ryoji Ito,*,† Ikumi Katano,* Miyuki Ida-Tanaka,* Tsutomu Kamisako,* Kenji Kawai,* Hiroshi Suemizu,* Sadakazu Aiso,† and Mamoru Ito*

Xenograft animal models using immunodeficient mice have been widely applied in medical research on various human diseases. NOD/Shi-*scid*-IL2rγ^{null} (NOG) mice are known to show an extremely high engraftment rate of xenotransplants compared with conventional immunodeficient mice. This high engraftment rate of xenotransplants in NOG mice was substantially suppressed by the transfer of spleen cells from NOD-*scid* mice that were devoid of NK cells. These results indicate that cell types other than splenic NK cells present in NOD-*scid* mice but not in NOG mice may be involved in this suppression. To identify the cell types responsible for this effect, we transferred subpopulations of spleen cells from NOD-*scid* mice into NOG mice and assessed the levels of human cell engraftment after human PBMC (hPBMC) transplantation. These experiments revealed that CD11c$^+$B220$^+$ plasmacytoid dendritic cells (pDCs) from NOD-*scid* mice markedly inhibited engraftment of human cells. The CD11c$^+$B220$^+$ CD122$^+$ cells further fractionated from the pDCs based on the expression of CD122, which is an NK cell marker strongly inhibited during hPBMC engraftment in NOG mice. Moreover, the CD122$^+$ cells in the pDC fraction were morphologically distinguishable from conventional CD122$^+$ NK cells and showed a higher rejection efficiency. The current results suggest that CD11c$^+$B220$^+$ CD122$^+$ cells play an important role in xenograft rejection, and their absence in NOG mice may be critical in supporting the successful engraftment of xenotransplants. *The Journal of Immunology*, **2012, 189: 4313–4320.**

We previously established the severely immunodeficient NOD/Shi-*scid*-IL2rγ^{null} (NOG) strain appropriate for generating a "humanized mouse" model in which human tissues, human cancers, and human PBMCs (hPBMCs) or cord blood hematopoietic stem cells (HSCs) can be engrafted or differentiated into multilineage immune cells after transplantation. Thus, these mice are useful as models for human tissue grafting (1, 2), cancer (3, 4), graft-versus-host disease (5), and the human immune system (6, 7). The success of xenoengraftment in NOG mice has been attributed to the multiple immunologic dysfunctions of acquired and innate immunity, whereby the lack of T and B cells and of NK cells is linked to the *scid* mutation (8) and to the IL-2 receptor common γ-chain deficiency (9), respectively.

The NOD strain in combination with the *scid* mutation or RAG deficiency is known to promote xenoengraftment. The recently reported signal regulatory protein-α (SIRP-α), which is a critical immune inhibitory receptor on macrophages, interacts with the CD47 ligand on the xenograft to prevent phagocytosis (10–12). Takenaka et al. (13) reported that the SIRP-α polymorphism on the NOD genetic background leads to enhanced binding to human CD47 and that this interaction may activate CD47-induced signaling pathways to support xenoengraftment. Furthermore, Shultz et al. (14) reported that complement-dependent hemolytic activity is more severely impaired in the NOD strain than in other inbred strains. These reports indicated that the NOD strain is much better than other strains in engrafting human cells and tissues. However, NOG mice showed a remarkably higher xenoengraftment level compared with NOD-*scid* mice despite having the NOD background. This higher xenoengraftment rate in NOG mice has been generally accepted as attributable to lack of NK cells as NOG mice lack NK cells through the introduction of an *IL-2Rγ* mutation. In fact, several reports have described how NK cells are important for xenograft rejection in immunodeficient mice. Higher success rates for xenoengraftment after transplantation of human HSCs were observed in NOD-*scid* β2m^{null} mice, which lack NK activity, and in NOD-*scid* mice treated with CD122 Ab than in nontreated NOD-*scid* mice (15–17). These results suggest that NK cells contribute to rejection of the transplanted xenograft. Conversely, our previous experiments have suggested that dendritic cells (DCs) might have a more pivotal role in xenograft rejection than NK cells. In our experiments, we found that the xenoengraftment level was significantly suppressed in NOD-*scid* mice treated with anti-NK Abs compared with NOG mice (6). Furthermore, we revealed that the production of inflammatory cytokines, such as IFN-γ and IL-6, was markedly reduced by spleen cells from NOG mice and CD11c$^+$ DC-depleted NOD-*scid* mice but not by those from NK cell-depleted NOD-*scid* mice (6). These results imply that the dysfunction of CD11c$^+$ DCs in NOG mice may be related to the high efficacy of xenoengraftment in these mice.

*Central Institute for Experimental Animals, Kawasaki-ku, Kawasaki, Kanagawa 210-0821, Japan; and †Department of Anatomy, Keio University School of Medicine, Shinjuku-ku, Tokyo 160-8582, Japan

Received for publication March 13, 2012. Accepted for publication August 29, 2012.

This work was supported by the Keio University Grant-in-Aid for Encouragement of Young Medical Scientists from Keio University School of Medicine and by a Grant-in-Aid for Young Scientists (B) (22700458) and for Scientific Research (S) (18100005) from the Ministry of Education, Culture, Sports, Science and Technology, Japan.

Address correspondence and reprint requests to Dr. Mamoru Ito, Central Institute for Experimental Animals, 3-25-12 Tonomachi, Kawasaki-ku, Kawasaki, Kanagawa 210-0821, Japan. E-mail address: mito@ciea.or.jp

The online version of this article contains supplemental material.

Abbreviations used in this article: BM, bone marrow; CIEA, Central Institute for Experimental Animals; DC, dendritic cell; hPBMC, human PBMC; HSC, hematopoietic stem cell; IKDC, IFN-producing killer dendritic cell; KO, knockout; mDC, myeloid dendritic cell; MNC, mononuclear cell; NOG, NOD/Shi-*scid*-IL2rγ^{null}; PB, peripheral blood; pDC, plasmacytoid dendritic cell; PI, propidium iodide; SIRP-α, signal regulatory protein-α.

www.jimmunol.org/cgi/doi/10.4049/jimmunol.1200820

DCs contribute to innate and adaptive immunity and act as professional APCs that are capable of Ag uptake, processing, and presentation to naive T cells (18, 19). DCs are classified into several populations based on surface markers and functional properties (20). Plasmacytoid dendritic cells (pDCs), characterized by the expression of CD11c and B220, represent a rare population of DCs that exists mainly in lymphoid tissues and plays a crucial role in producing type I IFNs against viruses via TLRs (21, 22). In transplant studies, prominent roles of DCs in graft rejection have been demonstrated using DC-depleted hosts (23). Thus, DCs may also suppress the reconstitution of donor cells and contribute to xenograft rejection.

In the current study, we investigated the role of DC subsets in hPBMC xenograft rejection using NOG mice. We performed transfer experiments with DC subpopulations and NK cells and demonstrated that $CD11c^+B220^+CD122^+$ cells, but not other DC subpopulations and NK cells obtained from NOD-*scid* mice, are potent inhibitors of hPBMC engraftment in NOG mice.

Materials and Methods

Ethics statement

All animal experiments were approved by the Institutional Animal Care and Use Committee of the Central Institute for Experimental Animals (CIEA) (certification number 11004A, February 16, 2011) and were performed in accordance with guidelines set forth by CIEA.

All experiments using human resources were approved by the Institutional Ethical Committee of the CIEA (certification number 08-11, September 4, 2008) and performed in accordance with CIEA guidelines. Written informed consent was obtained from all subjects in the current study.

Mice

NOD/Shi-*scid*-IL2rγ^{null} (NOG; formal name, NOD.Cg-*prkdc*^{scid}*il2rg*^{tm1Sug}/Jic) mice were bred and maintained under specific pathogen-free conditions at the CIEA. NOD.CB17-*prkdc*^{scid}/ShiJic (NOD-*scid*) mice were purchased from Clea Japan (Tokyo, Japan). NOD-*scid* EGFP transgenic mice were established by backcross mating of NOG-EGFP transgenic mice (24) to NOD-*scid* mice. IFN-γ knockout (KO) mice were kindly provided by Dr. Y. Iwakura (The University of Tokyo, Tokyo, Japan) and backcrossed with NOD-*scid* mice to establish the NOD-*scid* IFN-γ KO mice. These mice were housed in sterilized cages and fed sterilized food and water ad libitum. These four strains of immunodeficient mice were used at the age of 8–12 wk.

Transplantation of hPBMCs

Human peripheral blood (PB) samples were obtained from healthy volunteers after acquiring their informed consent. hPBMCs were isolated by Ficoll-Hypaque (GE Healthcare, Little Chalfont, Buckinghamshire, U.K.) density centrifugation and washed with PBS. Cells were resuspended in PBS and transplanted via the tail vein into NOG mice.

Isolation and transplantation of DC subpopulations and NK cells

The method used for isolating DC subpopulations has been described previously (25). Briefly, spleens from NOD-*scid*, NOG, or NOD-*scid* IFN-γ KO mice were minced and digested with 0.1% collagenase (Roche Diagnostics, Laval, QC, Canada) and DNase (1 mg/ml; Sigma-Aldrich, St. Louis, MO) at 37°C for 30 min. After washing with 2% FCS in PBS, the RBCs were lysed in Pharm Lyse buffer (BD Biosciences, San Jose, CA), and cells were stained with biotinylated mouse B220 Ab (BioLegend, San Diego, CA). To isolate DC subpopulations, cells were incubated with anti-biotin magnetic beads (Miltenyi Biotec, Sunnyvale, CA), and the $B220^+$ and $B220^-$ fractions were separated on a MACS column (Miltenyi Biotec). For myeloid dendritic cell (mDC) and pDC fractionation, the $B220^-$ cells were further reacted with anti-mouse CD11c magnetic beads (Miltenyi Biotec), and $CD11c^+$ cells were separated on a MACS column. The enriched $B220^+$ cells were almost all $CD11c^+$, as these mice lack B cells. For pDC and $CD11c^+B220^+CD122^+$ cell purification, the enriched $B220^+$ fractions were stained with PE-labeled mouse CD11c Ab (BioLegend), PE–Cy7–labeled streptavidin (BioLegend), and FITC-labeled mouse CD122 Ab (BD Biosciences). The $CD11c^+B220^+CD122^+$ cells and $CD11c^+B220^+CD122^-$ pDCs were sorted using the MoFlo cell sorter (Beckman Coulter, Stanford, CA), and the results were analyzed using FlowJo software (Tomy Digital Biology, Tokyo, Japan). The purity levels of the isolated mDC and pDC fractions ranged from 91 to 95% (MACS sorting), and those of the isolated pDCs and $CD11c^+B220^+CD122^+$ cells ranged from 97 to 99% (MoFlo sorting). NK cells, which were designated as $CD11c^-B220^-CD122^+$ cells, were isolated from the $B220^-$ cell fraction at >97% purity using the MoFlo cell sorter.

The purified mDCs, pDCs, $CD11c^+B220^+CD122^+$ cells, and NK cells were resuspended in PBS, and 1×10^5 to 2×10^5 cells were transplanted intravenously into NOG mice 1 d before hPBMC transplantation.

Flow cytometry

Bone marrow (BM), PB, and spleen samples were obtained from mice 2–7 wk after transplantation with hPBMCs. RBCs were lysed using the Pharm Lyse buffer (BD Biosciences), and mononuclear cells (MNCs) were prepared as single-cell suspensions. MNCs were incubated for 30 min at 4°C in the dark with the appropriate Abs. The following Abs were used: allophycocyanin–Cy7–labeled human CD45, PE- and allophycocyanin-labeled mouse CD11c, PE–Cy7–labeled mouse B220, PE-labeled mouse Siglec-H, PDCA-1, and Ly49D, and allophycocyanin-labeled mouse DX5 (BioLegend). After washing with 2% FCS in PBS, the MNCs were suspended in propidium iodide (PI) solution (BD Biosciences), followed by multicolor flow cytometry (FACSCanto; BD Biosciences) and analysis of the results using FACSDiva software (BD Biosciences). The rates of human leukocyte engraftment are expressed as the percentage of human $CD45^+$ ($hCD45^+$) cells in the PI^- total MNC population.

Cytotoxicity measurements

Cytotoxic activity was examined using the [^{51}Cr] release cytotoxic assay with Yac-1 target cells (kindly provided by Dr. K. Takeda, Juntendo University, Tokyo, Japan), according to the methods described by Shultz et al. (14). Briefly, NOD-*scid*, nontransplanted NOG mice, and NOG mice transplanted with pDCs or mDCs from NOD-*scid* mice were i.p. inoculated with polyinosinic-polycytidylic acid (Sigma-Aldrich) 48 h before assaying. Splenic MNCs from these mice were cocultured with ^{51}Cr-labeled Yac-1 target cells for 4 h at 37°C in a 5% CO_2 incubator with various E:T cell ratios. Each sample was prepared in triplicate, and the culture supernatants harvested from each well were assayed in a γ-counter (ARC300; Aloka, Tokyo, Japan). The percentage specific [^{51}Cr] release was calculated using the formula: percentage specific release = $[(X - S)/(T - S)] \times 100$, where X is the mean experimental release of [^{51}Cr] measured in triplicate wells. Total release (T) was determined from wells with ^{51}Cr-labeled Yac-1 cells and 1 N HCl, and spontaneous release (S) was determined from wells with ^{51}Cr-labeled Yac-1 cells and medium.

Induction of IFN-γ from DCs in vitro

In vitro IFN-γ induction was determined according to the methods described by Vremec et al. (25). Briefly, magnetically sorted pDC and mDC fractions were cultured in RPMI 1640 medium (Invitrogen, Carlsbad, CA) that contained 10% FCS in 96-well flat-bottom plates at 37°C in 5% CO_2. To induce IFN-γ, cells were stimulated with 5 ng/ml IL-12p70 (R&D Systems, Minneapolis, MN) and 20 ng/ml IL-18 (R&D Systems) or with 10 ng/ml PMA (Sigma-Aldrich) and 1 μg/ml ionomycin (Sigma-Aldrich) for 48 h. Culture supernatants were collected and stored at −80°C until use. IFN-γ was assayed using the Mouse IFNγ Quantikine ELISA Kit (R&D Systems).

Morphological analysis

pDCs, $CD11c^+B220^+CD122^+$ cells, and NK cells were isolated as described earlier. For May–Grünwald Giemsa staining, the enriched subpopulations were precipitated onto silane-coated glass slides (Muto Pure Chemicals, Tokyo, Japan) by cytospinning and were then air dried for 3 min. The slides were soaked in May–Grünwald solution (Muto Pure Chemicals) for 3 min and washed under running water to remove extra stain. The slides were further stained with 0.5% Giemsa solution (Muto Pure Chemicals) for 15 min. After washing with running water, the slides were dried and subjected to microscopic analyses.

Area and perimeter measurements of these smeared cells were automatically calculated using ImageJ 1.45s software (National Institutes of Health, Bethesda, MD).

Statistical analysis

Mean values and standard deviations were computed using Excel (Microsoft, Redmond, WA). Significant differences were calculated by Student t tests

and shown as $*p < 0.05$ and $**p < 0.005$. A p value <0.05 was deemed to be statistically significant.

Results

Suppression of human cell engraftment by the CD11c$^+$B220$^+$ pDC fraction

To investigate the effects of DCs on xenograft rejection, we first isolated two distinct DC fractions, CD11c$^+$B220$^+$ (pDCs) and CD11c$^+$B220$^-$ (mDCs), from NOD-*scid* and NOG mice, respectively. These two DC fractions were intravenously transplanted into NOG mice before hPBMC transplantation (Fig. 1A). The efficacy of successful hPBMC engraftment in PB, BM, and spleens from NOG DC-transplanted NOG mice and NOD-*scid* mDC-transplanted NOG mice was at the same level as that of non-transplanted control NOG mice. In contrast, hPBMC engraftment was completely suppressed in the PB, BM, and spleens of NOD-*scid* pDC-transplanted NOG mice at 7 wk posttransplantation (Fig. 1B). Spleen cells from the NOD-*scid*, NOD-*scid* pDC-transplanted or mDC-transplanted NOG, and untreated NOG mice without hPBMC transplantation were cocultured with Yac-1 target cells that were labeled with [^{51}Cr], then [^{51}Cr] release into the culture supernatants was measured. Although cytotoxicity was less effective compared with spleen cells of NOD-*scid* mice, those from the pDC-transplanted NOG mice showed a higher level of cytotoxicity compared with mDC-transplanted NOG and non-transplanted NOG mice (Fig. 1C). These results show that the high level of engraftment of NOG mice is suppressed by the NOD-*scid* pDC fraction, indicating that this fraction includes cells that mediate xenograft rejection.

NK marker-expressed cells in the pDC fraction have the potential for xenograft rejection

To identify cells that play critical roles in graft rejection, we used NOD-*scid* mice that systemically expressed GFP (NOD-*scid* EGFP Tg), and transplanted the pDC and mDC fractions isolated from the mice into NOG mice before hPBMC transplantation. At 7 wk posttransplantation, engraftment of hCD45$^+$ cells was inhibited in BM and spleens of the pDC-transplanted NOG mice (Fig. 2A, *top left panel*), consistent with the results shown in Fig. 1B. Also, GFP$^+$ cells were detected in the spleens of the pDC-transplanted NOG mice but not in those of the mDC-transplanted NOG mice (Fig. 2A, *top right panel*), and these GFP$^+$ cells expressed the DX5 Ag (Fig. 2A, *bottom panel*). These GFP$^+$DX5$^+$ cells might be expanded by recognizing xenografts and are considered to be responsible for their rejection. CD11c$^+$B220$^+$DX5$^+$ cells are known to produce high levels of IFN-γ upon stimulation (26, 27). We compared the levels of IFN-γ production of the isolated DC subpopulations from the spleen cells of NOD-*scid* and NOG mice. After stimulation with either IL-12 plus IL-18 or PMA plus ionomycin, high-level production of IFN-γ was observed in the pDCs from the NOD-*scid* mice but not in those from the NOG mice (Fig. 2B). We compared the expression of Siglec-H, PDCA-1, and CD122 on CD11c$^+$B220$^+$ cells between NOD-*scid* and NOG mice. pDCs generally express Siglec-H and PDCA-1 (28, 29) but not CD122, which is an NK cell marker and often used for detection of DX5 (30). Siglec-H and PDCA-1 were expressed on all CD11c$^+$B220$^+$ cells in the spleen of NOG mice, but CD122$^+$ cells were not observed (Fig. 2C). However, ~30% of CD11c$^+$B220$^+$CD122$^+$ cells were present in the spleens of NOD-*scid*

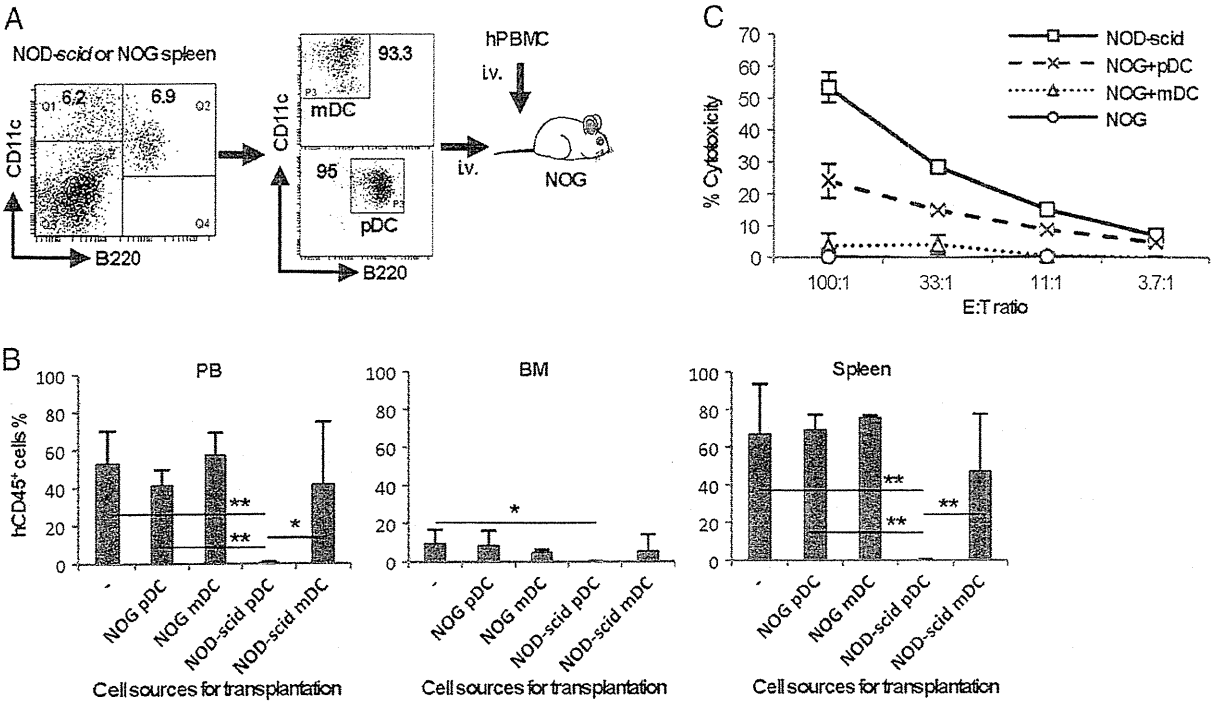

FIGURE 1. Suppression of xenoengraftment by the pDC fraction. (**A**) CD11c$^+$B220$^+$ pDCs and CD11c$^+$B220$^-$ mDCs from the spleens of NOD-*scid* and NOG mice were isolated using magnetic beads and MACS columns. These DC fractions (2×10^5 cells) were intravenously transplanted into NOG mice. At 1–2 d posttransplantation of the pDC or mDC fraction, 5×10^6 hPBMCs were intravenously transplanted into the NOG mice. (**B**) Engraftment of hCD45$^+$ cells is significantly inhibited in the PB, BM, and spleens of NOD-*scid* pDC-transplanted NOG mice ($n = 5$) but not in the PB, BM, and spleens of mDC-transplanted NOG mice ($n = 4$), and engraftment is not inhibited in nontreated NOG mice ($n = 3$) and NOG DC-transplanted NOG mice ($n = 3$) at 7 wk after hPBMC transplantation. (**C**) Spleen cells from NOD-*scid* (square plot), NOD-*scid* pDC-transplanted (cross plot), or mDC-transplanted (triangle plot) NOG mice and from untreated NOG mice (circle plot) were cocultured in triplicate with ^{51}Cr-labeled Yac-1 cells at various ratios for 4 h. Spleen cells from pDC-transplanted NOG mice showed high cytotoxicity compared with those from mDC-transplanted NOG mice. $*p < 0.05$, $**p < 0.005$.

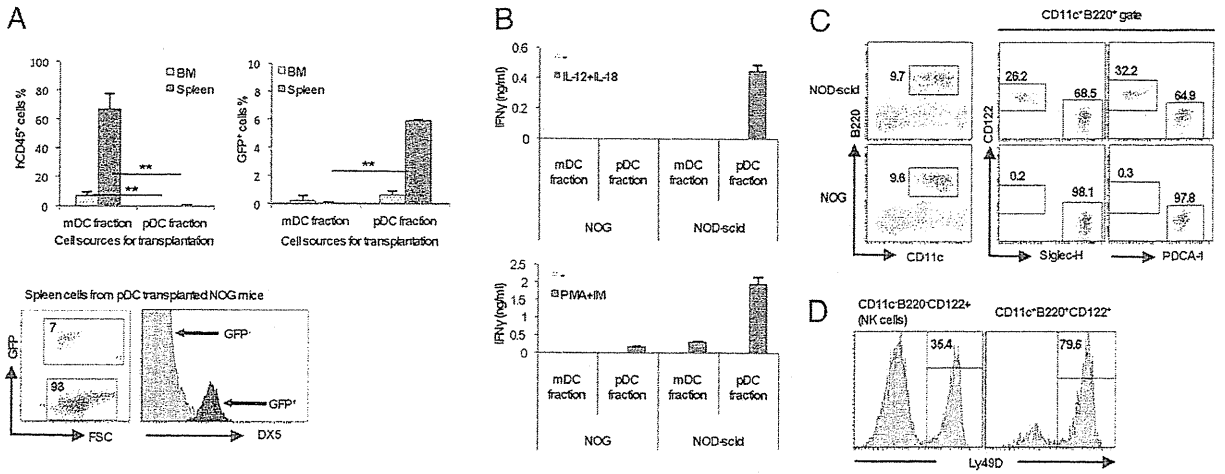

FIGURE 2. NK marker-expressed cells in the pDC fraction have the potential for xenograft rejection. (**A**) The pDC or mDC fraction from NOD-*scid* EGFP Tg mice was transplanted (2×10^5 cells) into NOG mice prior to transplantation with 5×10^6 hPBMCs, and the engrafted human cells and transplanted GFP^+ mouse cells were analyzed by flow cytometry at 7 wk posttransplantation. Engraftment of $hCD45^+$ cells was evident in the mDC-transplanted NOG mice ($n = 3$) but not in the pDC-transplanted NOG mice ($n = 3$). The percentage of engrafted mouse cells that expressed GFP was higher in the pDC-transplanted NOG mice than in the mDC-transplanted NOG mice. All the engrafted GFP^+ cells expressed the DX5 Ag. (**B**) The mDC or pDC fraction was isolated from NOD-*scid* or NOG mice, and 1×10^5 cells were cultured in duplicate with or without IL-12 plus IL-18 (*upper panel*) or PMA plus ionomycin (PMA+IM; *lower panel*). IFN-γ was strongly produced from the NOD-*scid* pDC fraction stimulated under both culture conditions. These assays were performed simultaneously, and the results are representative of three independent experiments. (**C**) Spleen cells from NOD-*scid* or NOG mice were stained with CD11c, B220, CD122, and Siglec-H or PDCA-1 Abs and analyzed by flow cytometry. $CD122^+$Siglec-H^- or $CD122^+PDCA\text{-}1^-$ cells were detected in the NOD-*scid* pDC fraction but not in the NOG pDC fraction. (**D**) Spleen cells from NOD-*scid* mice were stained with CD11c, B220, CD122, and Ly49D Abs. The histogram shows the frequencies of Ly49D expression on $CD11c^-B220^-CD122^+$ NK cells (*left*) and on $CD11c^+B220^+CD122^+$ cells (*right*). Similar results were obtained in three independent experiments (C, D). $^{**}p < 0.005$.

mice. We further analyzed Ly49D expression on $CD11c^+B220^+$ $CD122^+$ cells in NOD-*scid* mice. Ly49D is a receptor on NK cells and mediates allograft rejection by recognition of MHC class I molecules (31, 32). The frequency of Ly49D expression on $CD11c^+B220^+CD122^+$ cells was higher compared with that on $CD11c^-B220^-CD122^+$ NK cells in the spleens of NOD-*scid* mice (Fig. 2D). These results suggest that $CD11c^+B220^+CD122^+$ cells have a high potency for xenograft rejection and their absence in NOG mice may lead to high-level engraftment of human cells.

$CD11c^+B220^+CD122^+$ cells suppress xenoengraftment in NOG mice

To determine whether $CD11c^+B220^+CD122^+$ cells inhibit the engraftment of human cells, we isolated $CD11c^+B220^+CD122^+$ cells or pDCs ($CD11c^+B220^+CD122^-$) from NOD-*scid* mice by cell sorting (Fig. 3A). It is well known that pDCs produce type I IFNs after treatment with a TLR9 ligand (25). We demonstrated that isolated pDCs could produce IFN-α; however, IFN-α was not produced by $CD11c^+B220^+CD122^+$ cells (Supplemental Fig. 1). $CD11c^+B220^+CD122^+$ cells or pDCs were transplanted into NOG mice prior to hPBMC transplantation (Fig. 3A). Engraftment of the $hCD45^+$ leukocytes was significantly suppressed in the PB, BM, and spleens of $CD11c^+B220^+CD122^+$ cell-transplanted NOG mice, whereas the pDC-transplanted NOG mice showed similar percentages of engrafted human leukocytes to the non-transplanted control NOG mice at 7 wk posttransplantation with hPBMCs (Fig. 3B). We also isolated pDCs or $CD11c^+B220^+$ $CD122^+$ cells from NOD-*scid* and NOD-*scid* IFN-γ KO mice and transplanted them into NOG mice. The percentages of engrafted human leukocytes in the PB, BM, and spleens were not reduced by $CD11c^+B220^+CD122^+$ cells from NOD-*scid* IFN-γ KO mice (Fig. 3C). These results revealed that $CD11c^+B220^+CD122^+$ cells play a crucial role in xenograft rejection via IFN-γ production.

Suppressive effects of $CD11c^+B220^+CD122^+$ cells and NK cells on xenoengraftment

The possible involvement of NK cells in xenograft rejection was examined because these cells produce IFN-γ and are defective in NOG mice. Thus, we compared the efficiencies of xenograft rejection for $CD11c^+B220^+CD122^+$ cells and $CD11c^-B220^-$ $CD122^+$ NK cells. $CD11c^+B220^+CD122^+$ cells and NK cells were sorted from the spleen cells of NOD-*scid* mice and intravenously transplanted (1×10^5 or 2×10^5 cells) into NOG mice before hPBMC transplantation (Fig. 4A). At 2 and 4 wk posttransplantation, the $CD11c^+B220^+CD122^+$ cells were found to suppress human cell engraftment more potently than NK cells when 2×10^5 cells were transplanted (Fig. 4B, *right panel*), although the $CD11c^+B220^+CD122^+$ cells and NK cells did not cause rejection when 1×10^5 cells were transplanted (Fig. 4B, *left panel*). In vitro cytotoxic assays showed that the killing activity of $CD11c^+B220^+CD122^+$ cells was slightly higher than that of NK cells and that it could be suppressed by treating cells with an anti-NKG2D blocking Ab (Supplemental Fig. 2). Overall, these results indicate that $CD11c^+B220^+CD122^+$ cells have a greater potential than NK cells to induce xenograft rejection.

$CD11c^+B220^+CD122^+$ cells are distinguishable from NK cells

Previously, Vosshenrich et al. (33) reported that B220 expression on NK cells was inducible after activation in vitro and in vivo, and they argued that activated NK cells show a phenotypic resemblance to the $CD11c^+B220^+CD122^+$ IFN-producing killer dendritic cells (IKDCs). In contrast, Guimont-Desrochers et al. (34) showed that NK cells did not acquire B220 expression after adoptive transfer. To clarify this inconsistency, we investigated whether the sorted NK cells upregulated B220 and CD11c molecules after adoptive transfer. Fig. 5A shows that transplanted $CD122^+$ cells did not acquire B220 expression in the spleens of NK cell-transplanted NOG mice, whereas a small amount of

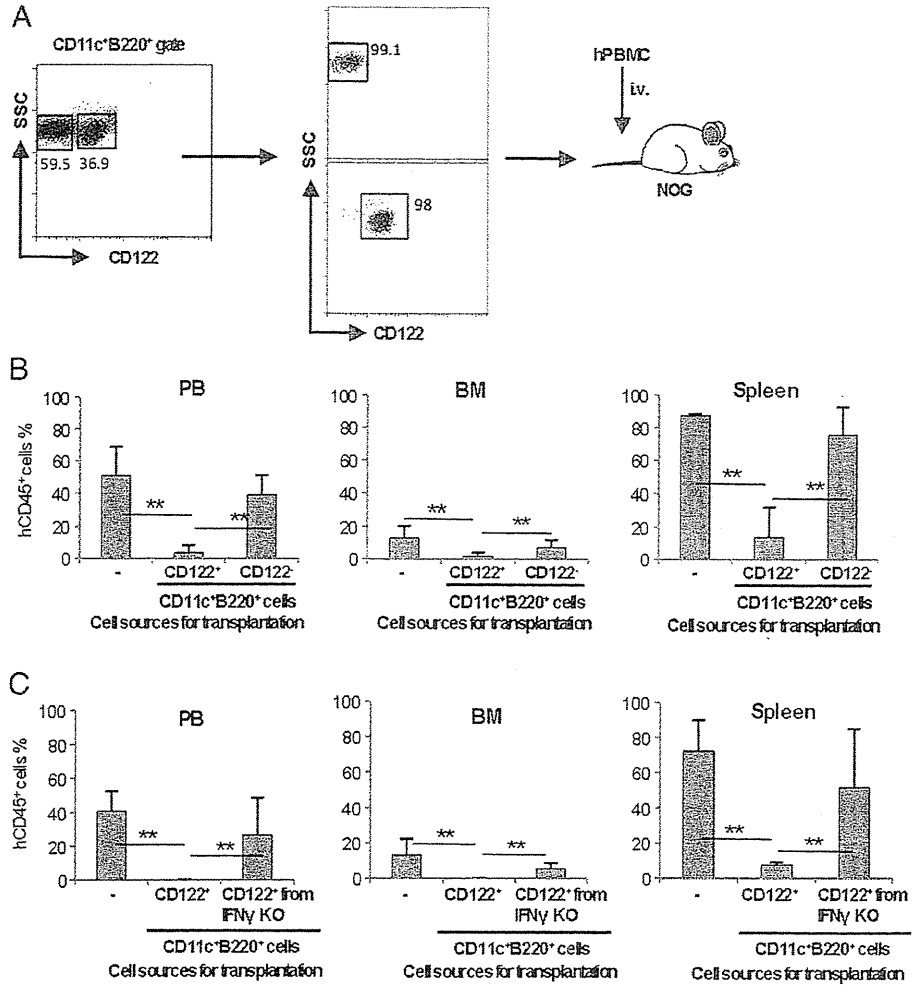

FIGURE 3. $CD11c^+B220^+CD122^+$ cells, but not pDCs, suppress xenoengraftment. (**A**) Scheme for the isolation of pDCs or $CD11c^+B220^+CD122^+$ cells using a MoFlo cell sorter and subsequent cell transfer (2×10^5 cells) into NOG mice before transplantation of hPBMCs (5×10^6 cells). (**B**) $hCD45^+$ human cell engraftment was analyzed by flow cytometry in the PB, BM, and spleens at 7 wk after hPBMC transplantation. The pDC-transplanted NOG mice ($n = 5$) showed a similar engraftment rate to that of the nontreated NOG ($n = 3$) mice, whereas a remarkable decrease in human cell engraftment was observed in the $CD11c^+B220^+CD122^+$ cell-transplanted NOG mice ($n = 5$). (**C**) $CD11c^+B220^+CD122^+$ cells from NOD-*scid* or NOD-*scid* IFN-γ KO mice were isolated and transplanted (2×10^5 cells) into NOG mice, followed by transplantation of 5×10^6 hPBMCs. The percentages of engrafted leukocytes were analyzed by flow cytometry at 6 wk posttransplantation. The percentage of $hCD45^+$ cells was inhibited in the PB, BM, and spleens of the NOD-*scid* $CD11c^+B220^+CD122^+$ cell-transplanted NOG mice ($n = 11$), whereas IFN-γ KO $CD11c^+B220^+CD122^+$ cells did not inhibit $hCD45^+$ cells as well as nontransplanted control NOG mice ($n = 6$). $^{**}p < 0.005$.

$CD122^+$ cells simultaneously expressed B220 and CD11c molecules in the spleens of $CD11c^+B220^+CD122^+$ cell-transplanted NOG mice. We further analyzed the morphological differences among sorted $CD11c^+B220^+CD122^+$ cells, NK cells, and pDCs by May–Giemsa staining. As observed in Fig. 5B, $CD11c^+B220^+CD122^+$ cells resembled pDCs; they showed a monocytic mor-

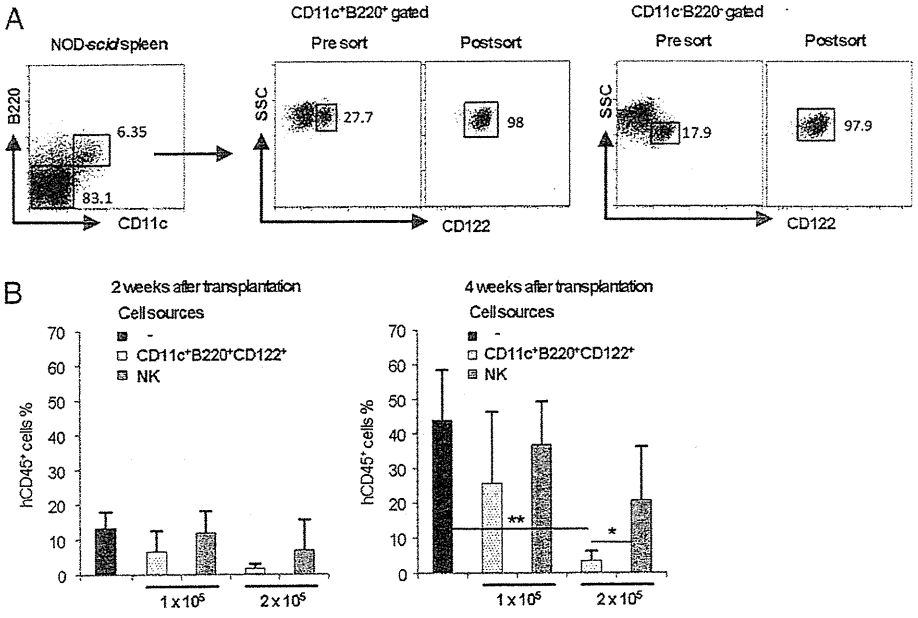

FIGURE 4. Suppressive effects of $CD11c^+B220^+CD122^+$ and NK cells on xenoengraftment. (**A**) $CD11c^+B220^+CD122^+$ cells or NK cells were positively isolated from the $CD11c^+B220^+$ fraction or $CD11c^-B220^-$ fraction of NOD-*scid* mice spleen cells using the MoFlo cell sorter, and 1×10^5 or 2×10^5 cells were transplanted into NOG mice before hPBMC transplantation. (**B**) At 2 and 4 wk posttransplantation, RBC-lysed PBMCs were collected from the transplanted NOG mice, and the efficacy of human cell engraftment was analyzed by flow cytometry. The percentage of engrafted $hCD45^+$ cells was significantly lower in the 2×10^5 $CD11c^+B220^+CD122^+$ cell-transplanted NOG mice ($n = 6$) than in the 2×10^5 NK cell-transplanted mice ($n = 7$). $^*p < 0.05$, $^{**}p < 0.005$.

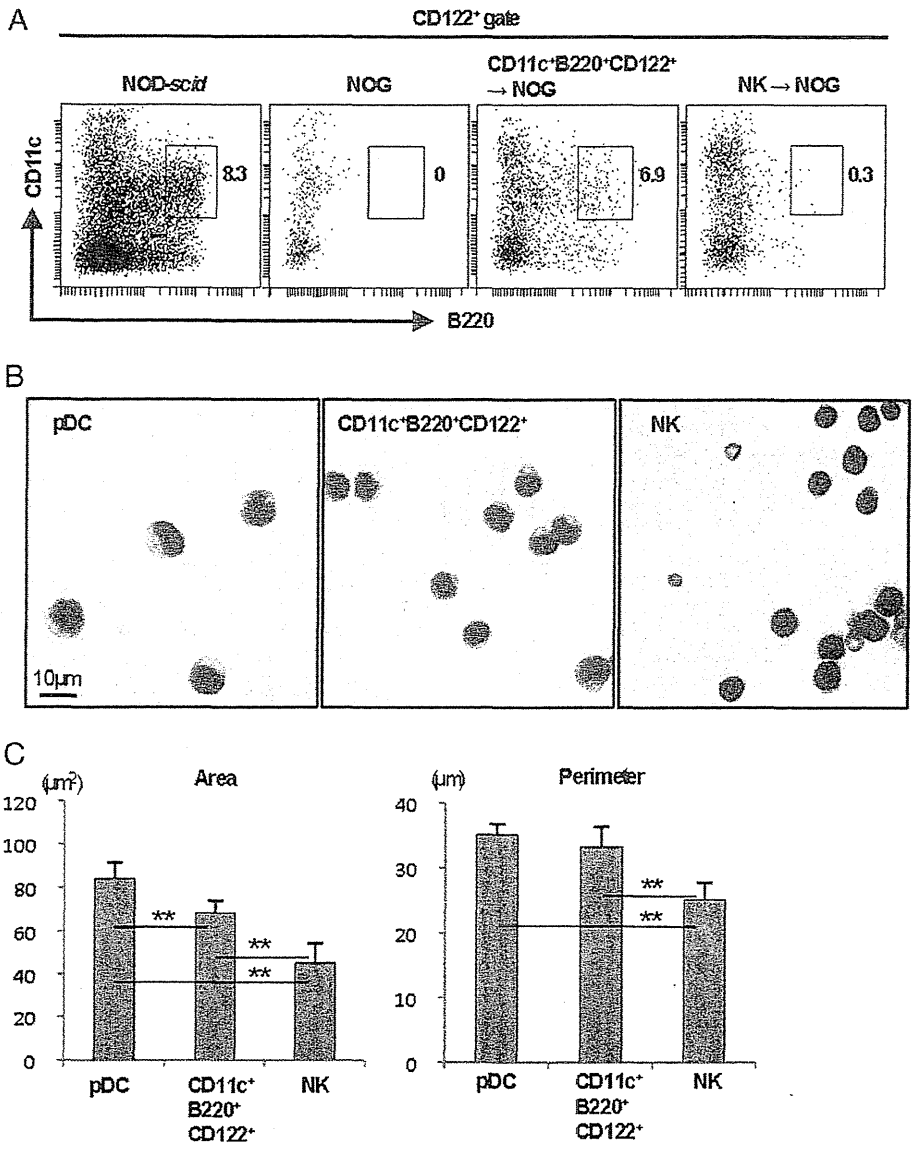

FIGURE 5. $CD11c^+B220^+CD122^+$ cells are distinguishable from NK cells. (**A**) $CD11c^+B220^+CD122^+$ or NK cells were purified using a MoFlo cell sorter, and 1×10^5 of these cells was transplanted into NOG mice. Two weeks after transplantation, spleen cells from the transplanted NOG, NOD-*scid*, and NOG mice were analyzed by flow cytometry. (**B**) Morphology of $CD11c^+B220^+CD122^+$ cells. Cytospin samples of sorted pDCs, $CD11c^+B220^+CD122^+$ cells, and NK cells were stained by May–Giemsa. (**C**) The means of the areas and perimeters of pDCs, $CD11c^+B220^+CD122^+$ cells, and NK cells were calculated using the ImageJ software. Similar results were obtained in two independent experiments. $^{**}p < 0.005$.

phology, low nuclear/cytoplasmic ratio, and dispersed chromatin. In contrast, NK cells showed a lymphocytic morphology, high nuclear/cytoplasmic ratio, and hyperchromatic nuclei. Moreover, we compared the area and perimeters of these cell populations using ImageJ analysis. $CD11c^+B220^+CD122^+$ cells had an intermediate area size between that of pDCs and NK cells and a larger perimeter than NK cells (Fig. 5C). These results demonstrated that $CD11c^+B220^+CD122^+$ cells were phenotypically and morphologically distinct from NK cells.

Discussion

In the current study, we investigated the mechanism underlying the high acceptance rate of xenografts in NOG mice. To determine the cells responsible for xenograft rejection, we transplanted DC subpopulations and NK cells from NOD-*scid* mice into NOG mice. We showed that the $CD11c^+B220^+CD122^+$ cells from NOD-*scid* mice strongly inhibited the engraftment of transplanted hPBMCs, whereas other DC subpopulations and NK cells from NOD-*scid* mice did not highly contribute to xenograft rejection in NOG mice. Throughout these experiments, we revealed that $CD11c^+B220^+CD122^+$ cells with characteristics commonly shared by IKDCs and activated NK cells—which are controversial cell lineages in xenograft rejection—are responsible for the rejection in immunodeficient mice.

A DC subpopulation that expresses NK cell markers CD122 and DX5 in the pDC fraction was identified as IKDCs, which share the functional properties and surface markers of DCs and NK cells and have cytotoxic activities and Ag-presenting abilities (35, 36). Taieb et al. (36) reported that IKDCs prevented transplanted tumor outgrowth and that IFN-γ–dependent and TRAIL-dependent killing activities and tumor recognition via MHC class II molecules occurred simultaneously when these cells were adoptively transferred, whereas conventional NK cells did not prevent these events. The authors claimed that IKDCs participate in tumor surveillance and act as effectors of innate immune responses. Regarding activated NK cells, $CD11c^+B220^+CD122^+$ cells more closely resemble NK cells than DCs (33, 37–39) because their developmental pathway is very similar to that of NK cells that rely on IL-15 signaling through the IL-2Rβ, IL-15Rβ, and common γ-chain. In our results, the $CD11c^+B220^+CD122^+$ cells resembled activated NK cells but not pDCs, as $CD11c^+B220^+CD122^+$ cells did not express Siglec-H and PDCA-1 and did not produce IFN-α